Supplementary Information for

A Scalable Stable Porous Coordination Polymer Synthesized from Low-cost Precursors for Efficient C_2H_2/C_2H_4 Separation

Hengcong Huang[#], Yifan Gu[#], Luyao Wang, Tao Jia, Susumu Kitagawa, Fengting Li[*]

Experimental Section

1. Materials and Synthesis

Nickel Nitrate Hexahydrate [$Ni(NO_3)_2·6H_2O$], methanol (MeOH), *N*,*N*-dimethylacetamide (DMA), *N*,*N*-dimethylformamide (DMF), ethanol (EtOH), nitric acid (HNO_3) and sodium hydroxide (NaOH) were purchased from Sinopharm Chemical Reagent Co., Ltd. 4-pyrazolecarboxylic acid (pca) and pyrazine (pyz) were purchased from WuXi AppTec Co., Ltd.

All chemicals and solvents were used without further purification. Deionized water was used throughout this work. N_2, CO_2, C_2H_2, C_2H_4, C_2H_6, and He were purchased from Air Liquide Co., Ltd with a purity of 99.99%.

Synthesis of TJE-1 single crystals. Firstly, 72.7 mg (0.25 mmol) $Ni(NO_3)_2·6H_2O$ and 28 mg (0.25 mmol) pca were dissolved in DMA/MeOH (1:1, 20 mL). Then, 20 mg (0.25 mmol) pyz was added to the above solution. Then the mixture was heated at 90 °C for 36 hours to yield green single crystal of TJE-1.

Conventional synthesis of TJE-1 microcrystalline samples. Firstly, 697.9 mg (2.4 mmol) $Ni(NO_3)_2·6H_2O$ and 268.8 mg (2.4 mmol) pca were dissolved in DMF/MeOH (1:1, 60 mL). Then, 192 mg (2.4 mmol) pyz were added to the above solution. Then the mixture was transferred to a 100 mL sealed vial and heated at 90 °C for 36 hours to yield TJE-1 microcrystalline samples. PXRD analysis results indicated that the as-synthesized powder is of the same phase as the single crystal of TJE-1. To obtain fully desolvated TJE-1, the as-synthesized samples were washed

three times with 10 mL methanol. The solvent was decanted and replaced with 10 mL of fresh MeOH twice a day for 5 days. Finally, the samples were dried under vacuum at 80 °C for 24 hours to obtain activated TJE-1. TGA analysis results indicated that all guest solvents were completely removed.

Scale-up synthesis of TJE-1. Firstly, 50.6 g (450 mmol) pca and 41.48 g (518 mmol) pyz were dissolved in DMF/MeOH (1:1, 9 L) in a 10 L sealed vessel. Then, 133.3 g (458 mmol) $Ni(NO_3)_2 \cdot 6H_2O$ was added to the above solution and dissolved. Then the mixture was heated at 80 °C for 36 hours to yield powder of TJE-1. The as-synthesized samples were washed three times with 1 L H_2O. The solvent was decanted and replaced with 5 L of fresh H_2O for 5 days and 2 L of MeOH for 2 days. Finally, the samples were dried under vacuum at 100 °C for 36 hours with a yield of 60.1 g (53.8% based on pca).

Explanation of use of solvents. DMF is a common solvent for the production of PCPs because the carboxylic acid groups in the ligands need to be deprotonated before they can be coordinated.[1] Solvents have been optimized in this study by using equal volumes of mixed DMF and MeOH instead of pure DMF. In the subsequent solvent exchange, water can be used to avoid the use of solvents such as acetone and dichloromethane.

2. General methods

Powder X-ray diffraction (PXRD) measurements were carried out with a Bruker D8 Advance X-Ray powder diffractometer (40 kV, 40 mA, Cu Kα1 radiation of λ = 1.54059 Å) at room temperature. The thermogravimetry analysis (TGA) curves were obtained from Water (Discovery TGA) at a constant rate of 5 °C/min from 50 °C to 500 °C in flowing N_2 gas. Scanning electron microscopic (SEM) images were taken on ZEISS Sigma 300 scanning electron microscope equipped with Oxford Xplore 30 energy dispersive X-ray spectrometer (EDX) system. X-ray photoelectron spectroscopic (XPS) experiments were carried out by Thermo Scientific K-Alpha using monochromatic Al Kα (*hv*=1486.6 eV). Binding energies were calibrated by using the containment carbon (C1s = 284.8 eV).

3. Single-crystal X-ray crystallography

Suitable crystals of as-synthesized TJE-1 were selected for single crystal X-ray data collections on a Bruker D8 VENTURE Metaljet PHOTON III diffractometer. The crystal was kept at 300.00 K during data collection. Using Olex2[2], the structure was solved with the SHELXT[3] structure solution program using Intrinsic Phasing and refined with the SHELXL[4] refinement package using Least Squares minimization. Crystallographic data and structural refinement summary are summarized in Table S2. Crystallographic data in CIF format have been deposited in the Cambridge Crystallographic Data Centre (CCDC) under deposition number CCDC-2181192. The data can be obtained free of charge via www.ccdc.cam.ac.uk/data_request/cif (or from the Cambridge Crystallographic Data Centre, 12 Union Road, Cambridge CB2 1EZ, U.K.).

4. Gas sorption isotherms and breakthrough experiments

The gas sorption curves of N_2, C_2H_2, C_2H_4, C_2H_6, and CO_2 were measured by BEL-max (Microtrac BEL Corp., Japan) gas adsorption instruments. Before all of the gas sorption and breakthrough separation experiments, samples were reactivated at 80 °C under vacuum for over 8 hours. Between each cycle of continuous C_2H_2 sorption measurements, the PCPs were regenerated by in situ vacuuming without heating. The temperatures of 77 K, 273 K, and 298 K were maintained with a liquid nitrogen bath or constant temperature water bath.

The Brunauer–Emmett–Teller (BET) surface areas and pore size distribution data were calculated from the N_2 adsorption isotherms at 77 K based on the BET method and Horvath–Kawazoe method (pore geometry: slit), respectively, in the BELMaster (ver. 7.3.1.0) software package.

The breakthrough experiments were carried out in BSD-MAB (Beishide Instrument Technology (Beijing) Co., Ltd.). In a conventional binary component experiment, 0.8 g of TJE-1 sample was packed into a stainless-steel column with an inner diameter of 6 mm and sample loading length of 58 mm. The column packed with samples was first purged with a flow of He (30 mL min^{-1}) at 80 °C for 2 h. Upon

cooling to 298 K, the equimolar C_2H_2/C_2H_4 gas mixture with a total flow rate of 2 mL min^{-1} was introduced to the column. For the scale-up synthesized sample experiment, ~56 g of TJE-1 sample was packed into a stainless-steel column with an inner diameter of 24.0 mm and sample loading length of 188 mm. Then the column was purged with He (10 mL min^{-1}) at 100 °C for 2 h and an equimolar C_2H_2/C_2H_4 gas mixture with a total flow rate of 10 mL min^{-1} was introduced to the column. Outlet effluent from the column was continuously monitored by an online mass spectrometry detector inside BSD-MAB.

The separation factor (*S*) of component 1 to component 2 is calculated by:

$$S = \left(\frac{X_1}{X_2}\right) \Big/ \left(\frac{Y_1}{Y_2}\right)$$

where X_1 and Y_1 are the molar fraction of component 1 in the adsorption phase and molar fraction of component 1 in the gas phase, respectively, X_2 and Y_2 are molar fraction of component 2 in the adsorption phase and molar fraction of component 2 in the gas phase, respectively.

The C_2H_4 productivity (*q*) is defined by the breakthrough amount of C_2H_4, which is calculated by integration of the breakthrough curves f(t) from t_1(18.55 min g^{-1}) to t_2(37.53 min g^{-1}) where the C_2H_4 purity >99.95%:

$$q = \frac{C_i(\mathrm{C_2H_4})}{C_i(\mathrm{C_2H_4}) + C_i(\mathrm{C_2H_2})} \times \int_{t_1}^{t_2} f(t)dt$$

For ternary components breakthrough experiment, generally, ~0.3 g of TJE-1 sample was packed into a stainless-steel column with an inner diameter of 4 mm and a sample loading length of 29 mm. The column packed with samples was first purged with a flow of He (20 mL min^{-1}) at 100 °C for 2 h. Upon cooling to 298 K, the C_2H_2/C_2H_4/X (X=CO or CO_2) (45/45/10,v/v/v) gas mixture with a total flow rate of 2 mL min^{-1} was introduced to the column. Outlet effluent from the column was continuously monitored by an online mass spectrometry detector inside BSD-MAB.

5. Stability test

To demonstrate the water stability of TJE-1, the activated 0.2 g TJE-1 was immersed in 20 mL water for 10 days. After that, the sample was filtered and dried under vacuum at 100 °C for 24 hours to obtain the reactivated sample. PXRD and C_2H_2 gas sorption curves of the reactivated TJE-1 were measured to reveal its water stability.

Moreover, to demonstrate the hot water stability of TJE-1, the activated 0.2 g TJE-1 was immersed in 20 mL water and then put in an oil bath at 80 °C. After 3 days, the samples were filtered and PXRD was measured to reveal its hot water stability.

To demonstrate the stability of TJE-1 in other situations, the activated 0.2 g TJE-1 was respectively immersed in 20 mL 0.1 M NaOH (pH=14), 0.01 M HNO_3 (pH=2), methanol, and ethanol for 10 days, or exposed to the air for 90 days. All the samples were filtered and PXRD was measured to reveal their stability.

6. Calculation of isosteric enthalpy of adsorption (Q_{st})

The below virial-type equation was used to fit the C_2H_2 and C_2H_2 adsorption isotherm data for TJE-1 at 273 and 298 K:

$$\ln P = \ln q + \frac{1}{T}\sum_{i=0}^{m} a_i q^i + \sum_{i=0}^{n} \binom{n}{k} b_i q^i$$

where P is the pressure (Pa), q is the adsorbed amount (mmol/g), T is the temperature (K), a_i and b_i are virial coefficients, and m and n are the numbers of coefficients used to describe the isotherms. The fitting parameters are summarized in Table S4.

Q_{st} is the coverage-dependent enthalpy of adsorption and is defined as:

$$Q_{st} = -R\sum_{i=0}^{m} a_i q^i$$

where R is the gas constant (8.314 J mol^{-1} K^{-1}).

7. Calculation of IAST selectivity

The selectivity for the adsorbate mixture composition was calculated from the single-component adsorption isotherms according to the ideal adsorbed solution

theory (IAST). First, the pure component isotherm data for C_2H_2 and C_2H_4 at 298 K were fitted to the dual-site Langmuir-Freundlich equation:

$$q = n_{m1}\frac{b_1 P^{(1/t_1)}}{1+b_1 P^{(1/t_1)}} + n_{m2}\frac{b_2 P^{(1/t_2)}}{1+b_2 P^{(1/t_2)}}$$

where q is the amount adsorbed per mass of material (mmol/g); P is the total pressure (kPa) of the bulk gas at equilibrium with the adsorbed phase; n_{m1} and n_{m2} are the saturation uptakes (mmol/g) for sites 1 and 2, respectively; b_1 and b_2 are the affinity coefficients (kPa^{-1}) for sites 1 and 2, respectively; and t_1 and t_2 represent the deviations from the ideal homogeneous surface (dimensionless) for sites 1 and 2, respectively. The fitted parameter values for C_2H_2 and C_2H_4 are presented in Table S3 with R^2 >0.999.

Finally, the selectivity for adsorbate i relative to adsorbate j was calculated using the following equation:

$$S_{i/j} = \frac{x_i y_j}{x_j y_i}$$

where x_i and x_j are the mole fractions of components i (C_2H_2) and j (C_2H_4) in the adsorbed phase in equilibrium, respectively, and y_i and y_j are the mole fractions of components i and j in the gas phase in equilibrium, respectively.

8. Calculation of separation potential

The separation potential (Δq) was calculated based on IAST by shock wave model[5, 6] :

$$\Delta q = q_{\mathrm{A}}\frac{y_{\mathrm{B}}}{1-y_{\mathrm{B}}}\left(1-\frac{1}{S_{\mathrm{A/B}}}\right)$$

where y_{B} is the mole fraction of C_2H_4 (B) entering the fixed bed and q_{A} is the uptake capacities of C_2H_2 (A) within the MOF that is in equilibrium with a bulk gas phase with partial pressures p_{A}. $S_{\mathrm{A/B}}$ is the IAST selectivity under the same conditions. Because the derivation of the separation potential Δq is based on an idealized shock wave model, it represents the maximum productivity of the ethylene that can be recovered.

9. DFT calculation

First-principles density functional theory (DFT) calculation was employed to describe the adsorption energies and function sites of C_2H_2 and C_2H_4 into TJE-1. The first principle calculations are performed by Vienna Ab initio Simulation Package(VASP) with the projector augmented wave (PAW) method.[7, 8] The exchange-functional is treated using the Perdew-Burke-Ernzerhof (PBE) functional, in combination with the DFT-D3 correction.[9] The calculations were performed in a spin-polarized manner. The cell parameters were a = 13.443 Å, b = 13.443 Å, c = 7.113 Å, α = 90.00°, β = 90.00°, γ = 90.00°, which are all consistent with the SCXRD results and demonstrated the accuracy of the calculation method. The cut-off energy of the plane-wave basis is set at 400 eV. For the optimization of both geometry and lattice size, the Brillouin zone integration is performed with 3*3*1 Monkhorts-Pack kpoint sampling.[10] The self-consistent calculations apply a convergence energy threshold of 10^{-5} eV. The equilibrium geometries and lattice constants are optimized with maximum stress on each atom within 0.02 eV/Å.

The binding energies (BE) of C_2H_2 and C_2H_4 with TJE-1 were calculated using:

$$BE = E\left(nG \subseteq \mathrm{PCP}\right)_{eq} - E\left(\mathrm{PCP}\right)_{eq} - nE\left(\mathrm{G}\right)_{eq}$$

where $E\left(nG \subseteq \mathrm{PCP}\right)_{eq}$ is the total energy of TJE-1 absorbed n gas molecules (G = C_2H_2 or C_2H_4) per unit cell, $E\left(\mathrm{PCP}\right)_{eq}$ and $E\left(\mathrm{G}\right)_{eq}$ are the total energies of empty TJE-1 and one free guest molecule, respectively, and the subscript “eq” represents the equilibrium state.

Table S1. Molecular size and boiling points of C_2H_2 and C_2H_4.[11, 12]

Gas	C_2H_2	C_2H_4
Molecular dimension (Å)	3.32×3.34×5.70	3.28×4.18×4.84
Boiling points (K)	188.4	169.4
Quadrupole moment ($\times10^{26}$ e.s.u. cm^2)	3.0	1.5
Polarizability ($\times10^{-25}$ cm^3)	33.3-39.3	42.5

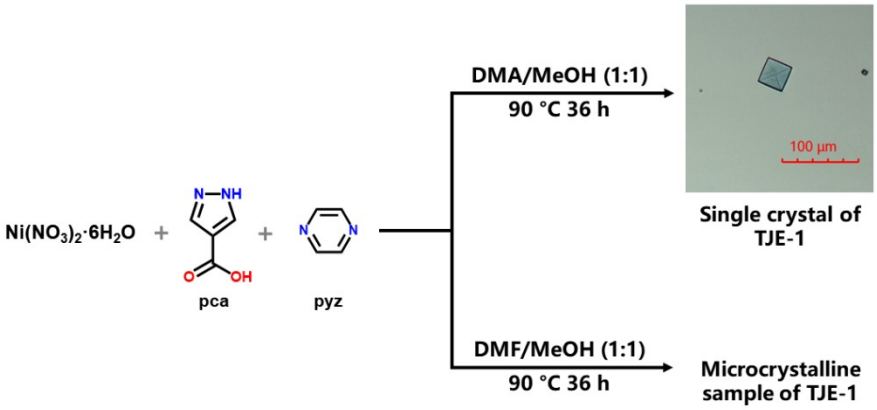

Figure S1. Scheme of synthesis of TJE-1 and photo of as-synthesized single crystals under a microscope.

Table S2. Crystallographic data and structural refinement summary for TJE-1.

Chemical formula	$C_8H_6N_4NiO_2$
Formula weight	248.88
Crystal system	tetragonal
Space group	*P*4/*mbm*
a (Å)	13.4433(11)
b (Å)	13.4433(11)
c (Å)	7.1126(11)
α (°)	90
β (°)	90
γ (°)	90
Volume (Å^3)	1285.4(3)
Z	4
Temperature (K)	300.00
μ (mm^{-1})	8.192
ρ_{calc} (g cm^{-3})	1.286
F(000)	504.0
Radiation	GaKα (λ = 1.34139)
Reflections collected	9875
Independent reflections	834
Goodness of fit	1.107
Final R indexes (I>=2σ (I))	R_1=0.0371, wR_2=0.1027
Final R indexes (all data)	R_1=0.0446, wR_2=0.1057

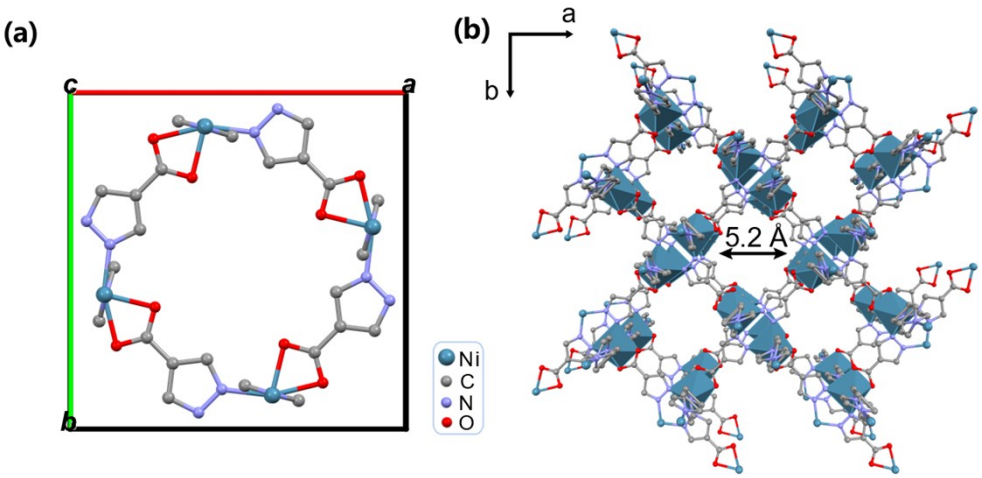

Figure S2. Crystal structures of TJE-1. (a) The unit cell of TJE-1 viewed along *c* axis. (b) Microporous channels in TJE-1 viewed along *c* axis (Color code: Ni, cyan; C, gray; N, blue; O, red; H atoms are omitted for clarity. Probe radius: 1.2 Å).

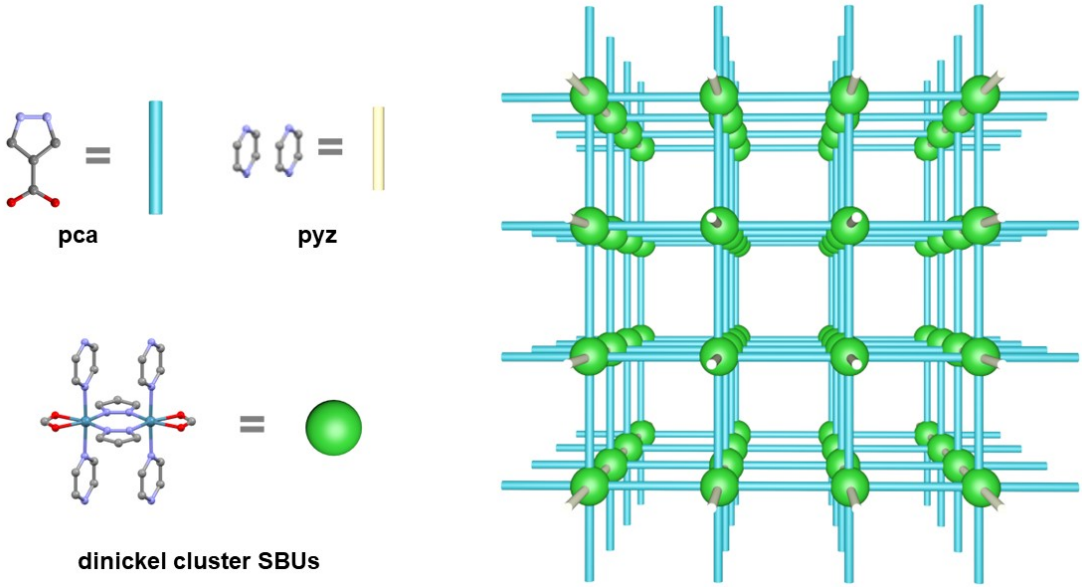

Figure S3. Schematic diagram of the network of TJE-1.

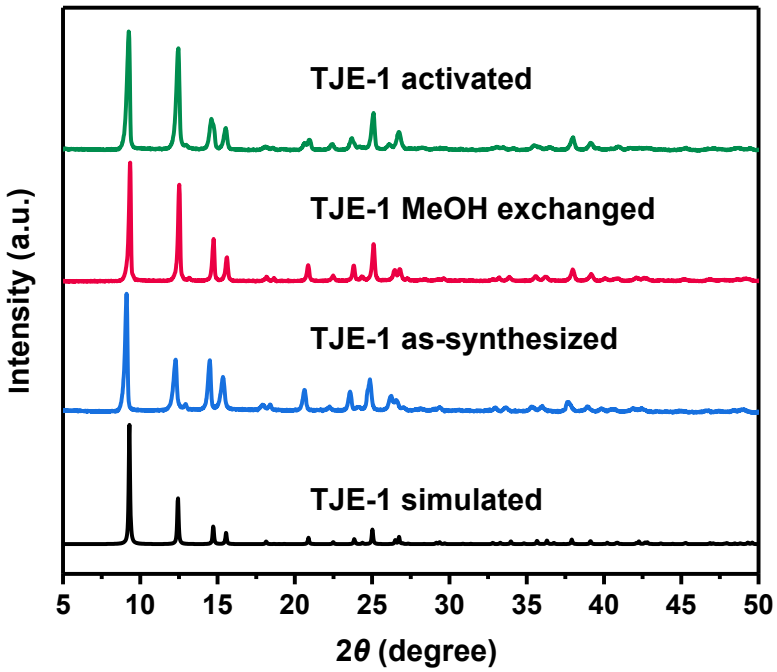

Figure S4. The powder X-ray diffraction (PXRD) patterns of TJE-1.

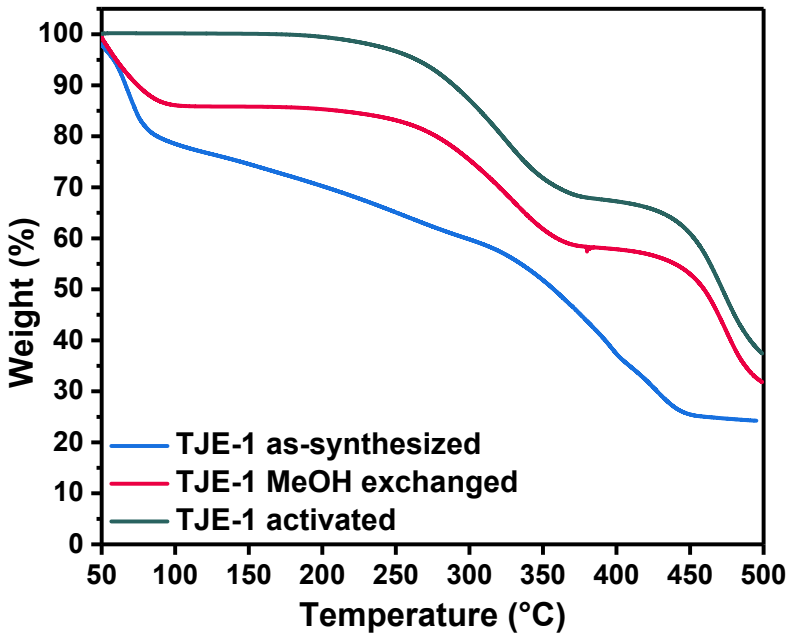

Figure S5. TGA analysis of as-synthesized, MeOH exchanged, and activated TJE-1.

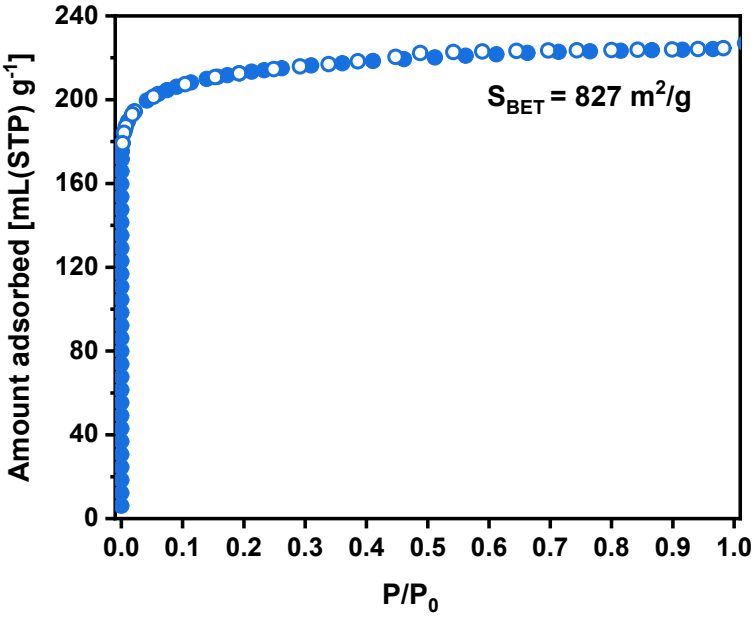

Figure S6. N_2 sorption isotherms at 77 K and the Brunauer–Emmett–Teller (BET) surface area of activated TJE-1.

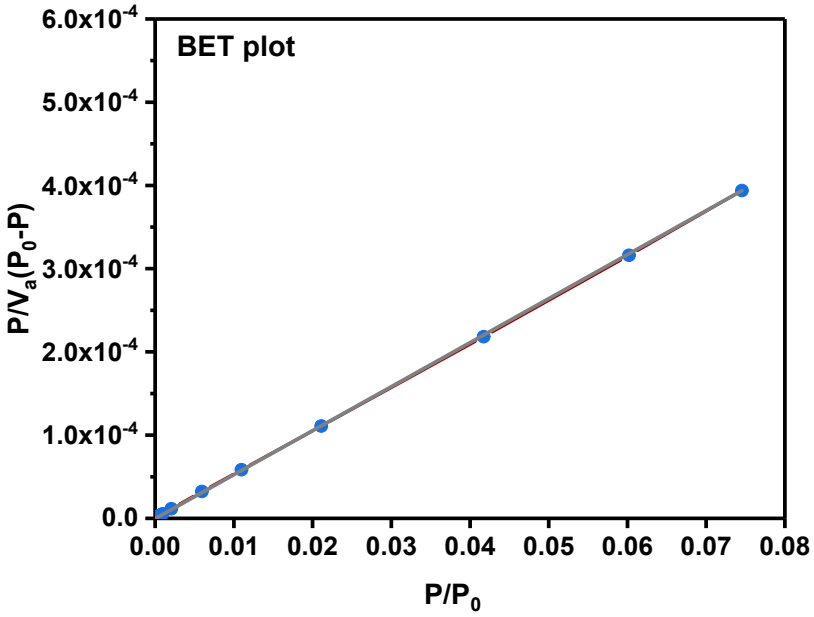

Figure S7. Brunauer–Emmett–Teller (BET) plot for surface area calculation of TJE-1 based on N_2 adsorption isotherm at 77 K. (*C* value, 470780; Correlation coefficient, 0.9999; BET surface area, 827 m^2 g^{-1}.)

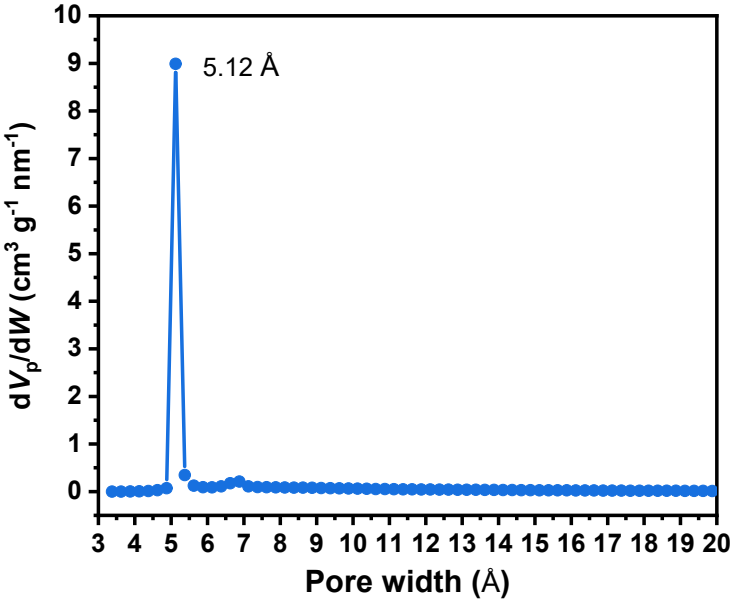

Figure S8. Pore size distribution (PSD) of TJE-1 based on the adsorption branch of N_2 adsorption isotherm at 77 K with Horvath–Kawazoe (HK) model.

Table S3. Fitting parameters for IAST selectivity calculation

	C_2H_2	C_2H_4
n_{m1}	3.2658	0.9387
n_{m2}	5.5776	5.7641
b_1	0.1726	0.1798
b_2	0.0148	0.0205
t_1	1.1185	0.7960
t_2	1.2001	1.3700
R^2	0.99997	0.99999

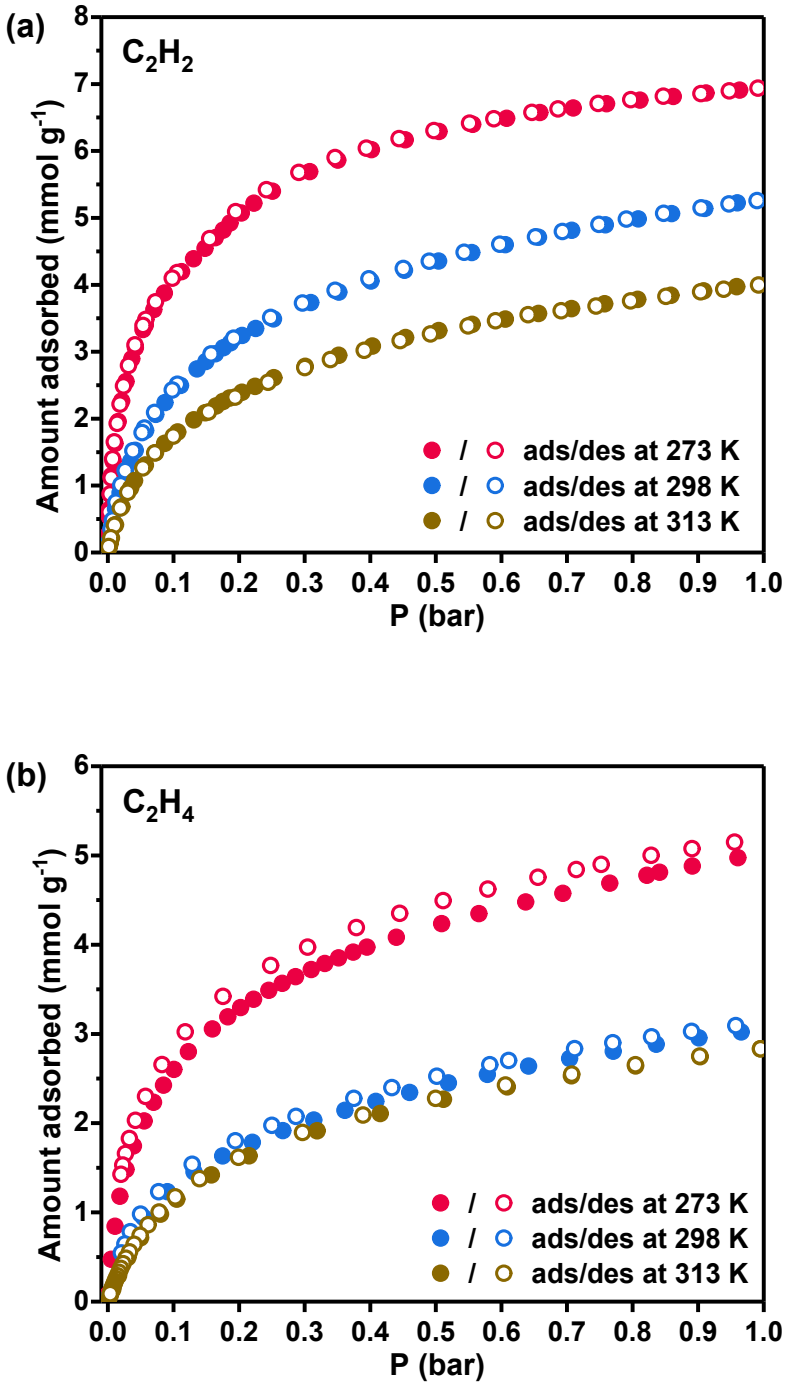

Figure S9. C_2H_2 (a) and C_2H_4 (b) sorption isotherms for TJE-1 at 273 K, 298 K and 313 K.

Table S4. Fitting parameters for Q_{st} calculation

	C_2H_2	C_2H_4
a_0	-4271.62596	-3520.15
a_1	105.53457	-1053.09
a_2	-181.26569	941.0122
a_3	39.72881	-338.514
a_4	-3.41244	33.82942
a_5	0.23188	-2.35015
b_0	21.47951	19.88806
b_1	0.08037	3.28655
b_2	0.56961	-2.03776
b_3	-0.08455	0.5999
R^2	0.99923	0.99303

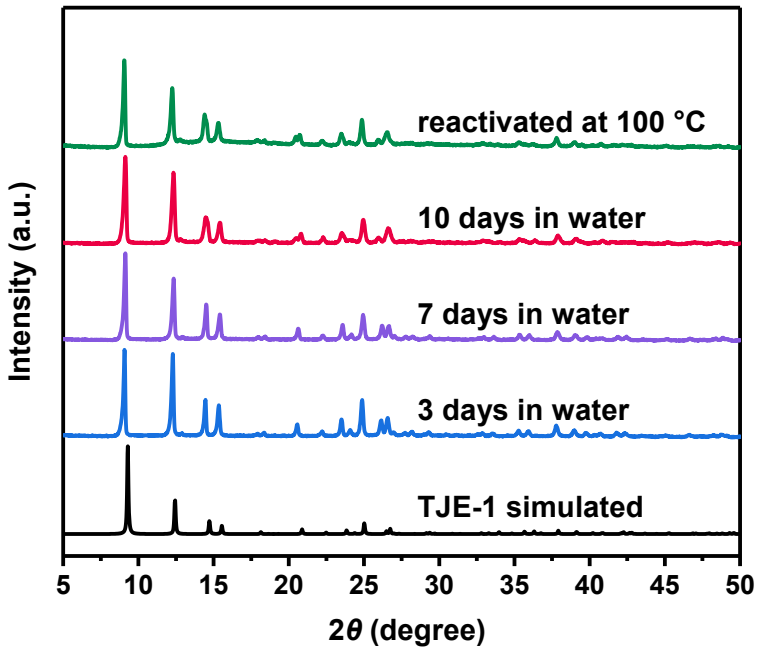

Figure S10. The powder X-ray diffraction (PXRD) patterns of TJE-1 after immersion in water for various time, showing the water stability of TJE-1.

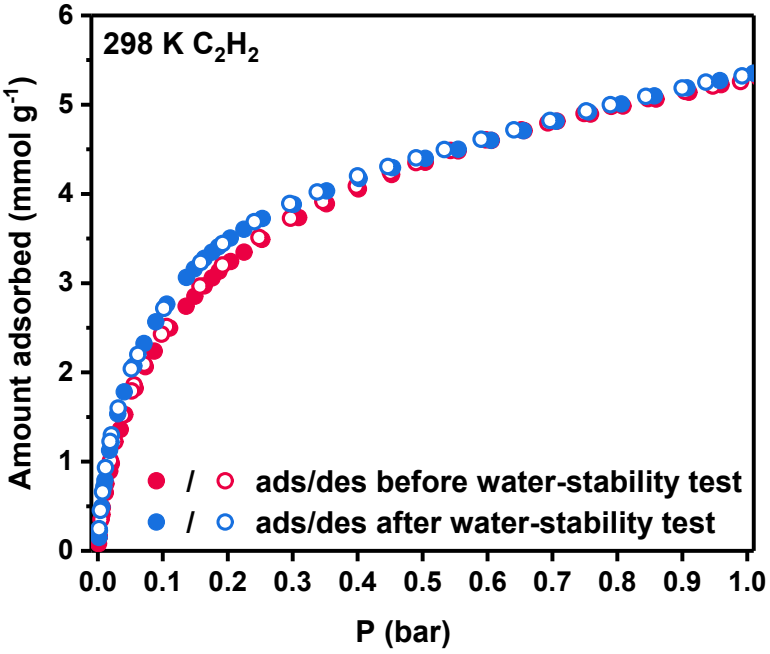

Figure S11. The C_2H_2 sorption for TJE-1 reactivated at 100 °C, recorded before and after immersion in water for 10 days. This indicates that the pore structure of TJE-1 remains stable in water.

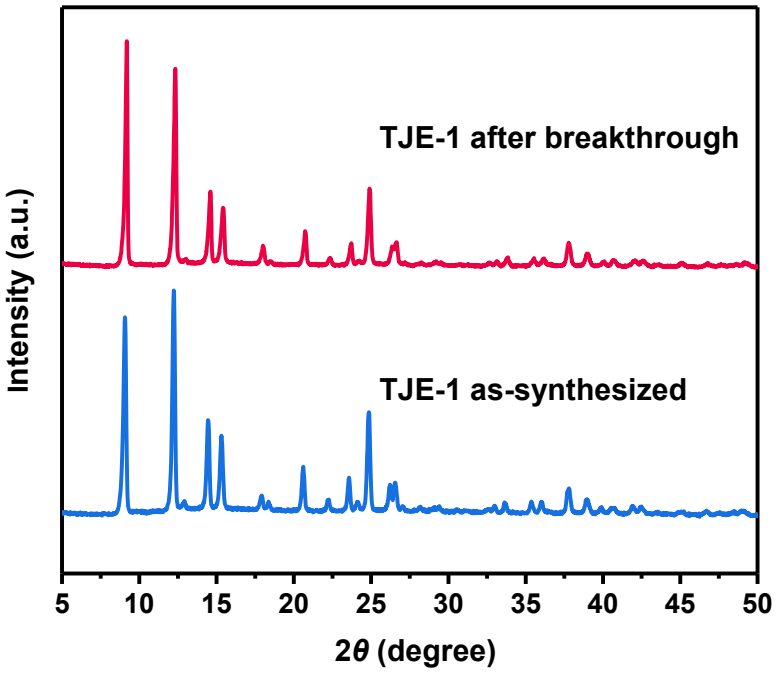

Figure S12. PXRD patterns of TJE-1 before and after the breakthrough experiment.

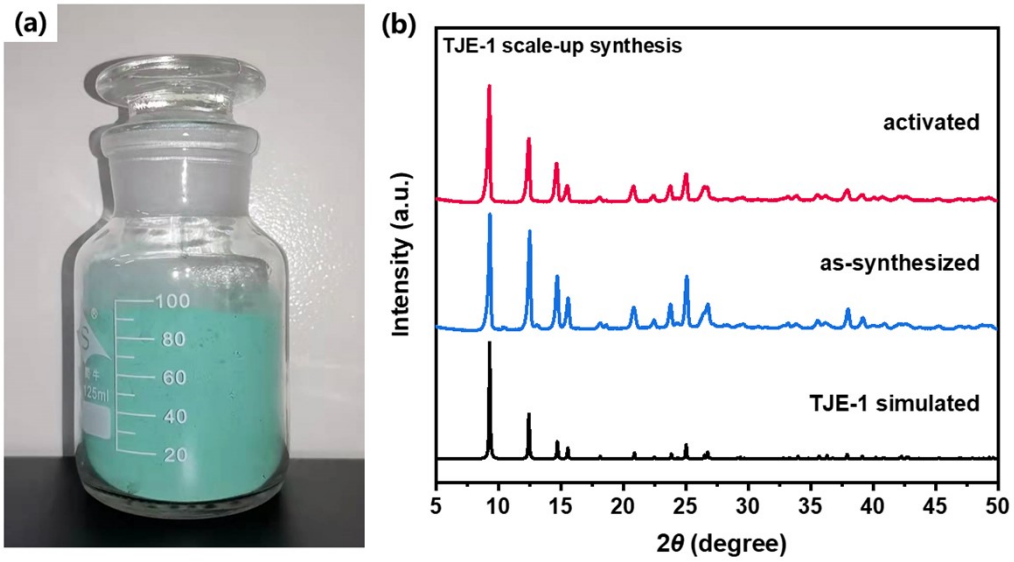

Figure S13. (a) Optical photo and (b) powder X-ray diffraction (PXRD) pattern of TJE-1 obtained by scale-up synthesis.

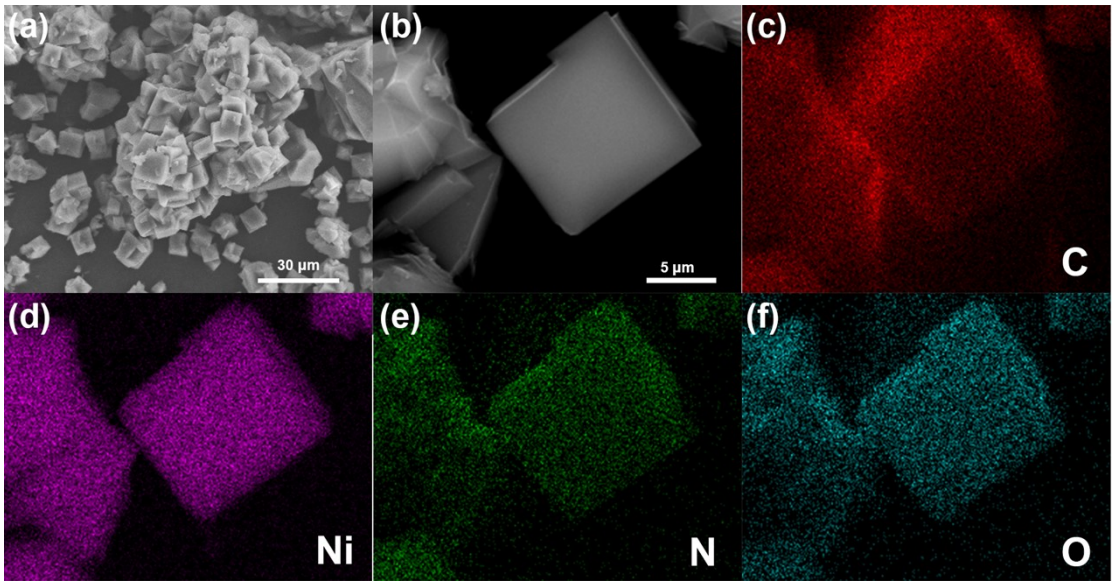

Figure S14. (a,b) SEM images of conventionally synthesized TJE-1 microcrystalline. (c-f) EDS mapping of a typical interface of TJE-1. The resolution of the EDS probe used is 16 nm ×16 nm.

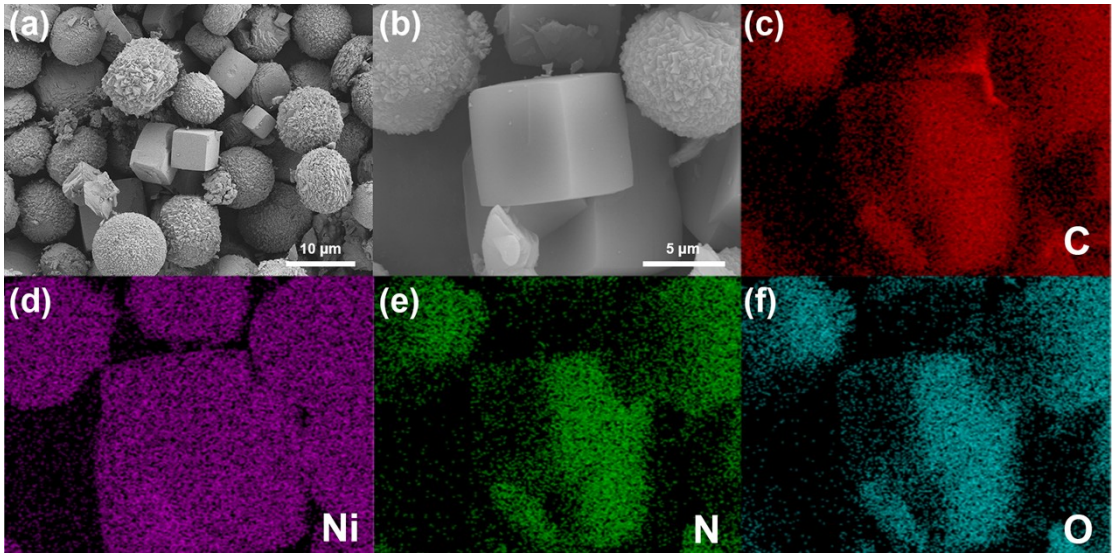

Figure S15. (a,b) SEM images of scale-up synthesized TJE-1 samples. (c-f) EDS mapping of a typical interface of TJE-1. The resolution of the EDS probe used is 16 nm ×16 nm.

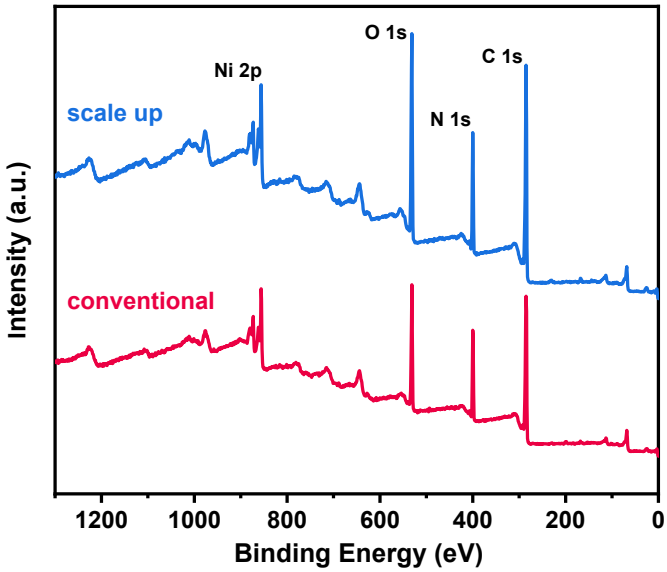

Figure S16. XPS survey spectrum of the conventionally synthesized and scale-up synthesized TJE-1.

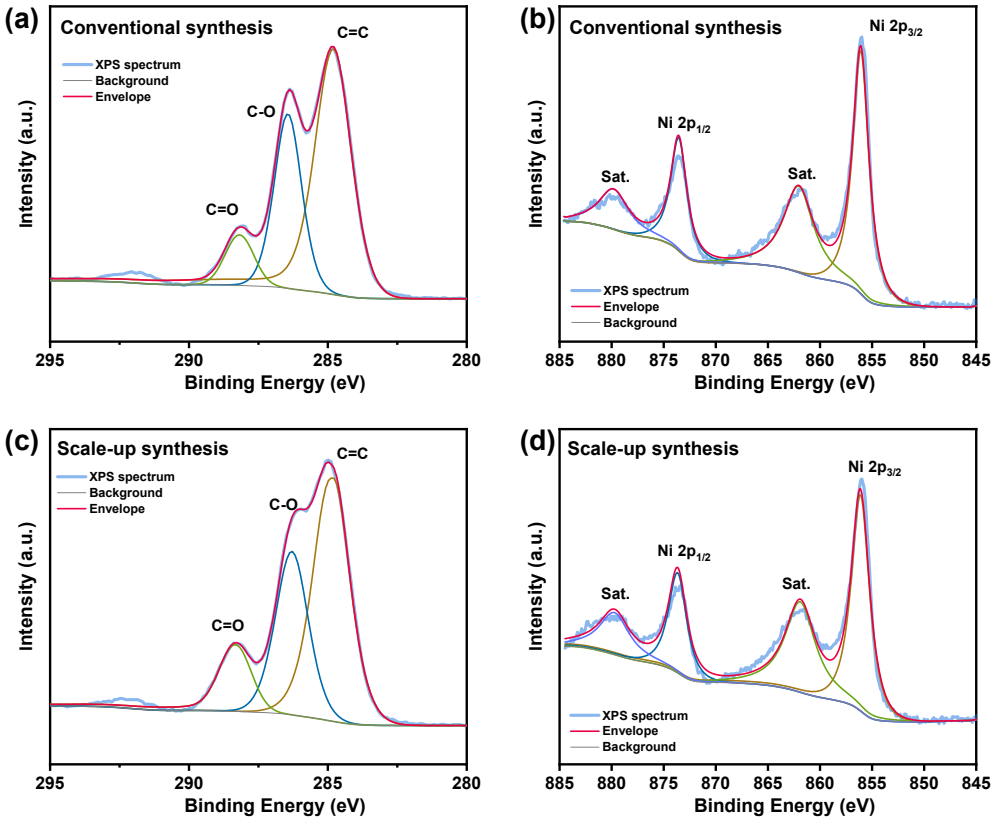

Figure S17. XPS spectra of the conventionally synthesized (a,b) and scale-up synthesized (c,d) TJE-1 in the C 1s and Ni 2p region.

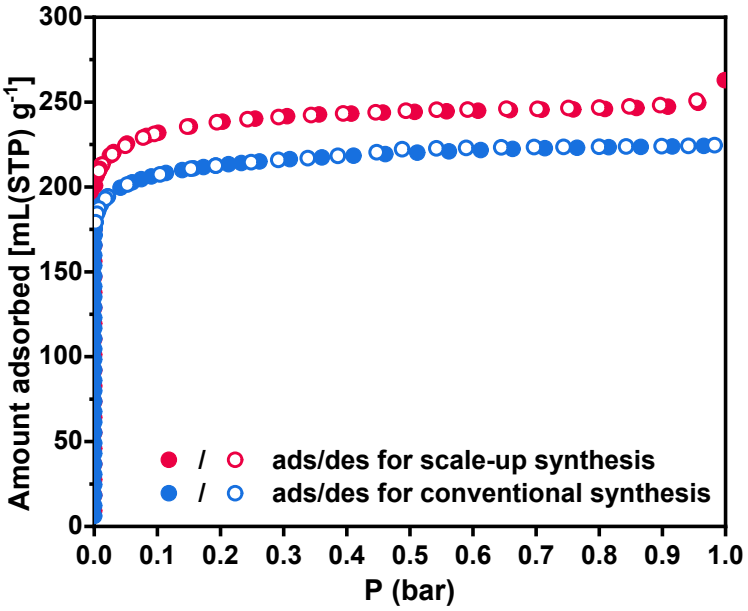

Figure S18. N_2 sorption isotherms at 77 K of scale-up synthesized TJE-1.

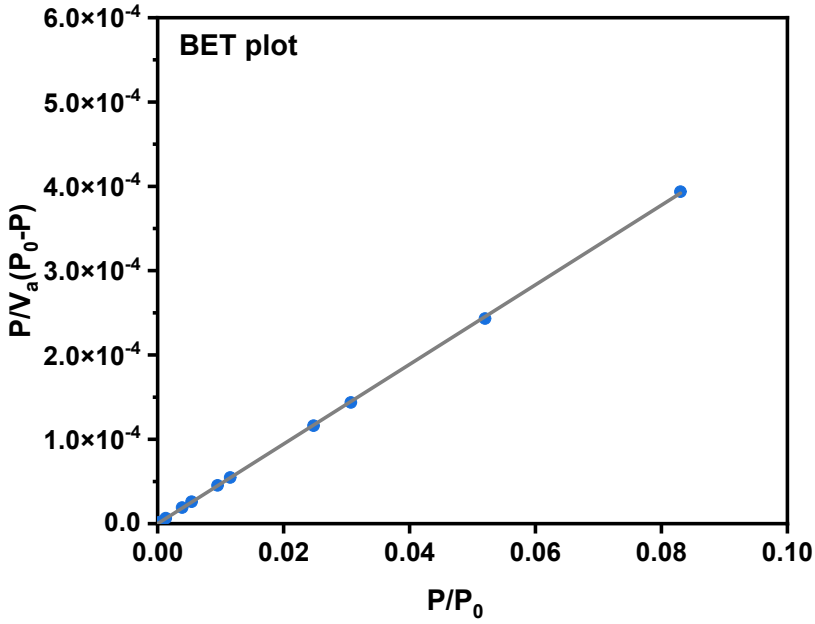

Figure S19. BET plot for surface area calculation of scale-up synthesized TJE-1 based on N_2 adsorption isotherm at 77 K. (*C* value, 104650; Correlation coefficient, 0.9999; BET surface area, 922 m^2 g^{-1}.)

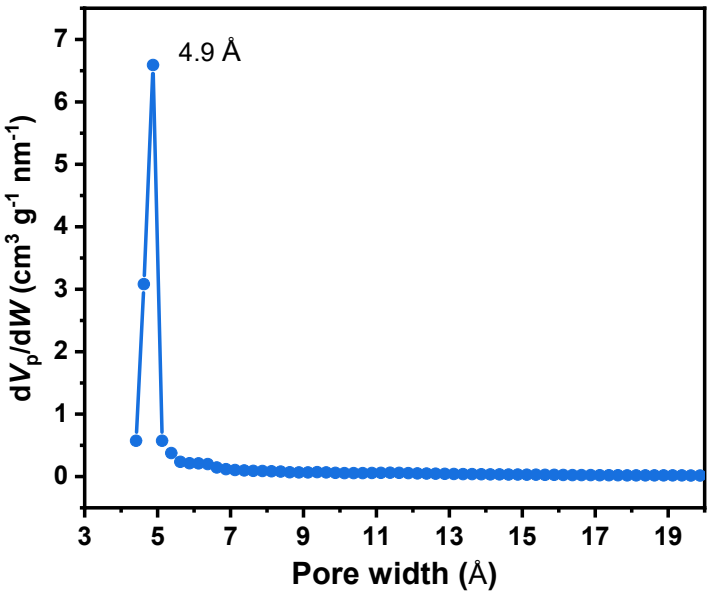

Figure S20. PSD of scale-up synthesized TJE-1 based on the adsorption branch of N_2 adsorption isotherm at 77 K with HK model.

Table S5. Comparison of the main precursor costs of TJE-1 and other PCPs for C_2H_2/C_2H_4 separation. *

PCPs	Main precursors (indicated by CAS number)	Commercial price ($ g^{-1})	Cost level	Ref.
UTSA-100	2015178-17-1	unavailable	very high	[13]
UTSA-200	2632-99-7	116[c]	high	[14]
UTSA-300	37968-97-1	113[b]	high	[15]
SIFSIX-1-Cu	553-26-4	0.7[a]	low	[16]
SIFSIX-3-Zn	290-37-9	0.13[a]	low	[16]
SIFSIX-3-Ni	290-37-9	0.13[a]	low	[16]
SIFSIX-2-Cu-i	73564-69-9	130[a]	high	[16]
Fe-MOF-74	610-92-4	4.8[a]	low	[17]
M'MOF-3a	1373442-99-9	unavailable	very high	[18]
NOTT-300	4371-28-2	117[a]	high	[19]
NKMOF-1-Ni	1236181-13-7	unavailable	very high	[20]
ZU-32	73564-69-9	130[a]	high	[21]
ZU-33	2632-99-7	116[c]	high	[21]
TIFSIX-2-Cu-i	73564-69-9	130[a]	high	[22]
TIFSIX-4-Cu-i	113682-56-7	70.6[a]	high	[22]
ZrT-1-tetrazol	1010915-67-9	300[a]	very high	[23]
NbU-1	73-24-5	0.2[a]	low	[24]
ZJU-74a	339527-86-5 and 290-37-9	1.5+0.13[a]	low	[25]
GeFSIX-dps-Cu	37968-97-1	113[b]	high	[26]
ZUL-100	37968-97-1	113[b]	high	[27]
ZUL-200	37968-97-1	113[b]	high	[27]
TJE-1	**37718-11-9 and 290-37-9**	**1.45+0.13[a]**	**low**	**This work**

* Only the main organic ligand precursors were listed. The commercial price of laboratory reagents is the lowest price in China collected in January 2023 from three different suppliers [WuXi AppTec Co. Ltd., Tokyo Chemical Industry (Shanghai) Co. Ltd., and Merck KGaA (China) Co. Ltd.] and converted to US dollars.

[a] Provided by WuXi AppTec Co. Ltd.

[b] Provided by Tokyo Chemical Industry (Shanghai) Co. Ltd.

[c] Provided by Merck KGaA (China) Co. Ltd.

Table S6. Comparison of TJE-1 and various benchmark PCPs for C_2H_2/C_2H_4 separation. *

PCPs	Functional Sites	C_2H_2 capacity (mmol g^{-1})	Selectivity	Δq (mol kg^{-1})	Q_{st} of C_2H_2 (kJ mol^{-1})	Water stability	Precursors cost	Ref.
UTSA-100	Free N site, $–NH_2$	4.27	10.72	3.87	22	moderate	very high	13
UTSA-200	Molecular sieving and SiF_6^{2-}	3.65	6320 [a]	3.65	40	moderate	high	14
UTSA-300	Molecular sieving	3.41 [b]	Molecular sieving	3.41 [b]	57.6 [b]	low	high	15
SIFSIX-1-Cu	SiF_6^{2-}	8.5	10.63	7.70	37	moderate	low	16
SIFSIX-3-Zn	SiF_6^{2-}	3.64	8.82	3.23	31	moderate	low	16
SIFSIX-3-Ni	SiF_6^{2-}	3.3	5.03	2.64	30.5	low	low	16
SIFSIX-2-Cu-i	SiF_6^{2-}	4.02	44.54	3.93	41.9	moderate	very high	16, 28
Fe-MOF-74	Open metal sites	6.8	2.08	3.53	47	low	low	17
M'MOF-3a	Molecular sieving	1.9	24.03	1.82	25	moderate	very high	18
NOTT-300	Supramolecular interactions	6.34 [c]	2.17 [c]	3.42 [c]	32	high	high	19
NKMOF-1-Ni	Open metal sites	2.72	1272.6	2.72	60.3	high	very high	20
ZU-32	GeF_6^{2-}	3.97	67	3.91	42.6	moderate	very high	21
ZU-33	GeF_6^{2-}	3.78	＞1100 [a]	3.78	56.6	moderate	high	21
TIFSIX-2-Cu-i	TiF_6^{2-}	4.1	55 [d]	4.03 [d]	46.3	low	very high	22
TIFSIX-4-Cu-i	TiF_6^{2-}	4.3	11 [d]	3.91 [d]	40.8	moderate	high	22
ZrT-1-tetrazol	tetrazole N hydrogen bond	2.58	4.08	1.95	33.27	high	very high	23
NbU-1	Open metal sites	2.72	5.9	2.26	38.3	high	low	24
ZJU-74a	Oen metal sites	3.39 [e]	24.2 [d,e]	3.25 [d,e]	45–65 [e]	high	moderate	25
GeFSIX-dps-Cu	Molecular Sieving	4.28	40.1 [f]	4.17	——	high	high	26
ZUL-100	TiF_6^{2-}	5.31	175 [d]	——	65.3	high	high	27
ZUL-200	$NbOF_5^{2-}$	4.69	114 [d]	——	57.6	high	high	27
TJE-1	**O sites, pyz ring**	**5.27**	**4.16**	**4.00**	**35.5**	**high**	**low**	**This work**

* Unless otherwise specified, the capacity data are all recorded at 1 bar, 298 K, and selectivity is IAST selectivity for 50/50 (v/v) C_2H_2/C_2H_4 mixtures. The separation potential (Δq) is for C_2H_2/C_2H_4 (50/50,v/v) at 1 bar, 298 K. Water stability is a qualitative comparison: moderate

stability means stable in humid air, high stability means stable after being soaked in water and low stability means water-sensitive. The precursors costs detail was shown in Table S5.

[a] The value is only for qualitative comparison.

[b] The data was collected at 273 K.

[c] The data was collected at 293 K.

[d] The data was for 1/99 (v/v) C_2H_2/C_2H_4 mixtures.

[e] The data was collected at 296 K.

[f] The data was derived from actual gas desorption processes.

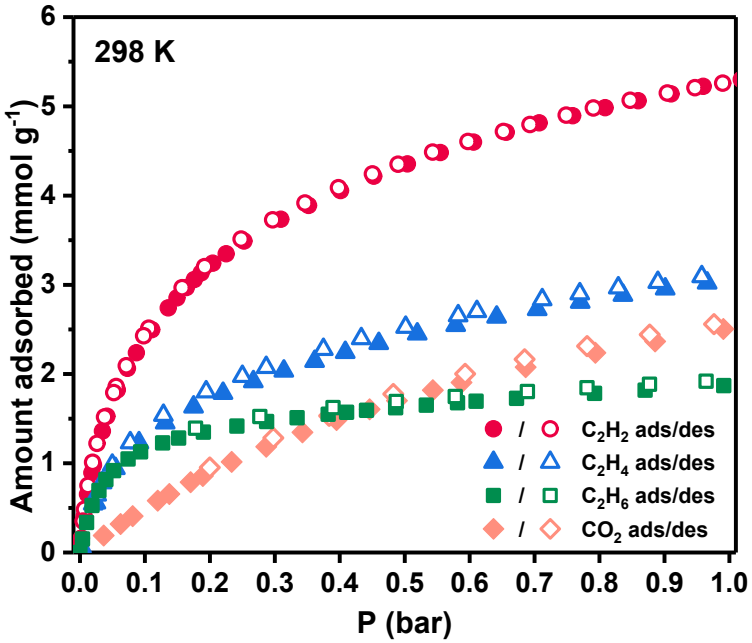

Figure S21. C_2H_2, C_2H_4, C_2H_6 and CO_2 sorption for TJE-1 at 298 K.

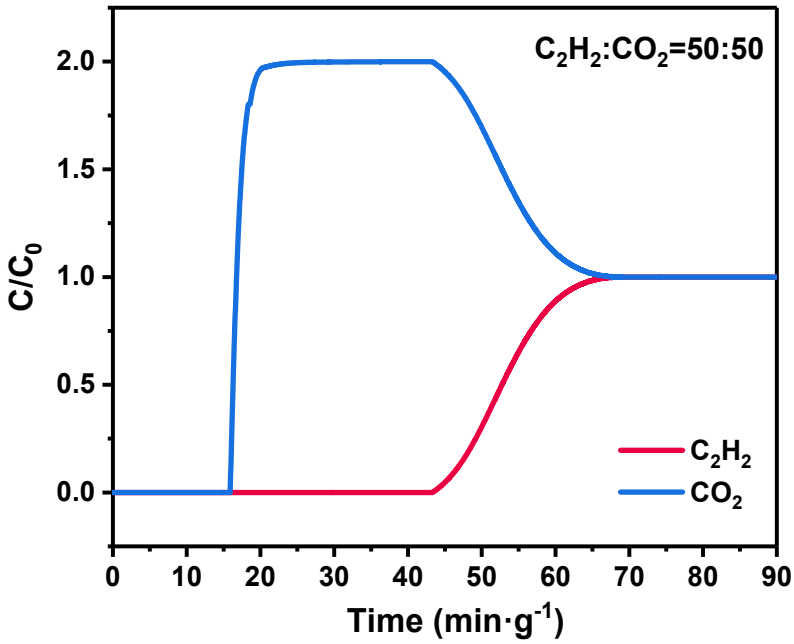

Figure S22. Experimental breakthrough curve of TJE-1 under total flow at 2 mL min^{-1} for an equimolar gas mixture of C_2H_2 and CO_2 at 298 K.

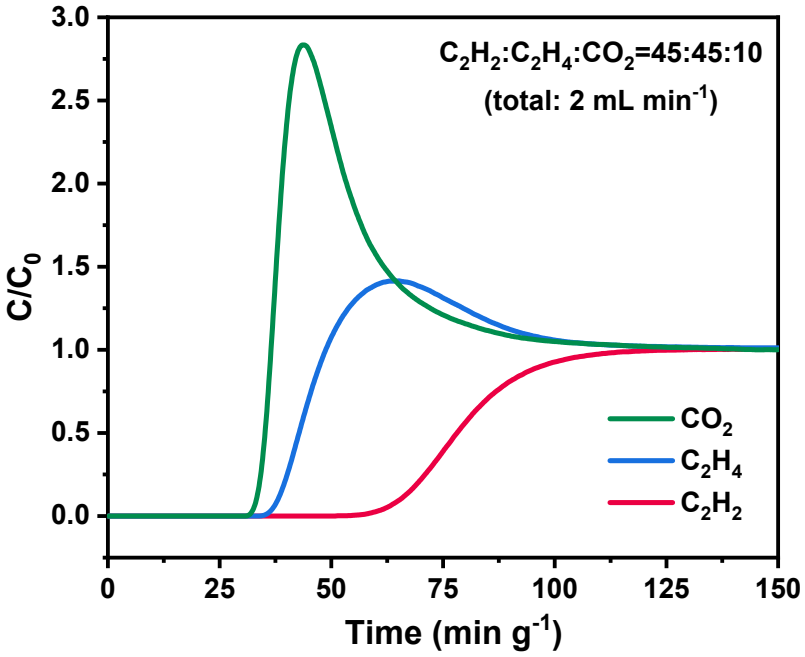

Figure S23. Experimental breakthrough curve of TJE-1 under total flow at 2 mL min^{-1} for $C_2H_2/C_2H_4/CO_2$ (45/45/10,v/v/v) gas mixture at 298 K.

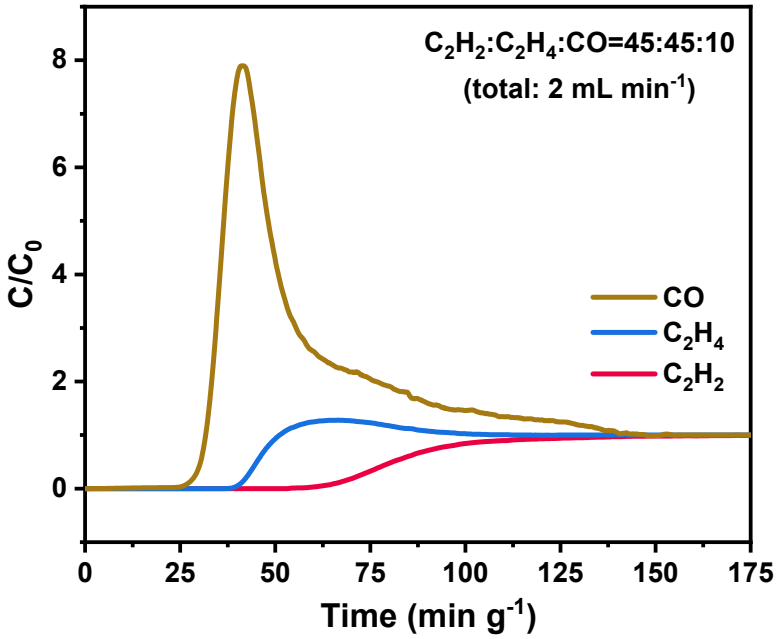

Figure S24. Experimental breakthrough curve of TJE-1 under total flow at 2 mL min^{-1} for $C_2H_2/C_2H_4/CO$ (45/45/10,v/v/v) gas mixture at 298 K.

Reference:

1. A. J. Howarth, A. W. Peters, N. A. Vermeulen, T. C. Wang, J. T. Hupp and O. K. Farha, *Chem. Mater.*, 2017, **29**, 26-39.
2. O. V. Dolomanov, L. J. Bourhis, R. J. Gildea, J. A. K. Howard and H. Puschmann, *J. Appl. Crystallogr.*, 2009, **42**, 339-341.
3. G. Sheldrick, *Acta Crystallographica, Section A*, 2015, **71**, 3-8.
4. G. Sheldrick, *Acta Crystallographica, Section C*, 2015, **71**, 3-8.
5. R. Krishna, *RSC Adv.*, 2017, **7**, 35724-35737.
6. R. Krishna, *ACS Omega*, 2020, **5**, 16987-17004.
7. J. P. Perdew, K. Burke and M. Ernzerhof, *Phys. Rev. Lett.*, 1996, **77**, 3865-3868.
8. G. Kresse and D. Joubert, *Physical Review B*, 1999, **59**, 1758-1775.
9. S. Grimme, J. Antony, S. Ehrlich and H. Krieg, *The Journal of chemical physics*, 2010, **132**, 154104.
10. H. J. Monkhorst and J. D. Pack, *Physical Review B*, 1976, **13**, 5188-5192.
11. S. Mukherjee, D. Sensharma, K.-J. Chen and M. J. Zaworotko, *Chem. Commun.*, 2020, **56**, 10419-10441.
12. L. Yang, S. Qian, X. Wang, X. Cui, B. Chen and H. Xing, *Chem. Soc. Rev.*, 2020, **49**, 5359-5406.
13. T.-L. Hu, H. Wang, B. Li, R. Krishna, H. Wu, W. Zhou, Y. Zhao, Y. Han, X. Wang, W. Zhu, Z. Yao, S. Xiang and B. Chen, *Nat. Commun.*, 2015, **6**, 7328.
14. B. Li, X. Cui, D. O'Nolan, H.-M. Wen, M. Jiang, R. Krishna, H. Wu, R.-B. Lin, Y.-S. Chen, D. Yuan, H. Xing, W. Zhou, Q. Ren, G. Qian, M. J. Zaworotko and B. Chen, *Adv. Mater.*, 2017, **29**, 1704210.
15. R.-B. Lin, L. Li, H. Wu, H. Arman, B. Li, R.-G. Lin, W. Zhou and B. Chen, *J. Am. Chem. Soc.*, 2017, **139**, 8022-8028.
16. X. Cui, K. Chen, H. Xing, Q. Yang, R. Krishna, Z. Bao, H. Wu, W. Zhou, X. Dong, Y. Han, B. Li, Q. Ren, M. J. Zaworotko and B. Chen, *Science*, 2016, **353**, 141-144.
17. D. Bloch Eric, L. Queen Wendy, R. Krishna, M. Zadrozny Joseph, M. Brown Craig and R. Long Jeffrey, *Science*, 2012, **335**, 1606-1610.
18. S.-C. Xiang, Z. Zhang, C.-G. Zhao, K. Hong, X. Zhao, D.-R. Ding, M.-H. Xie, C.-D. Wu, M. C. Das, R. Gill, K. M. Thomas and B. Chen, *Nat. Commun.*, 2011, **2**, 204.
19. S. Yang, A. J. Ramirez-Cuesta, R. Newby, V. Garcia-Sakai, P. Manuel, S. K. Callear, S. I. Campbell, C. C. Tang and M. Schröder, *Nat. Chem.*, 2015, **7**, 121-129.
20. Y.-L. Peng, T. Pham, P. Li, T. Wang, Y. Chen, K.-J. Chen, K. A. Forrest, B. Space, P. Cheng, M. J. Zaworotko and Z. Zhang, *Angew. Chem. Int. Ed.*, 2018, **57**, 10971-10975.
21. Z. Zhang, X. Cui, L. Yang, J. Cui, Z. Bao, Q. Yang and H. Xing, *Ind. Eng. Chem. Res.*, 2018, **57**, 7266-7274.

22. A. Bajpai, D. O'Nolan, D. G. Madden, K.-J. Chen, T. Pham, A. Kumar, M. Lusi, J. J. Perry, B. Space and M. J. Zaworotko, *Chem. Commun.*, 2017, **53**, 11592-11595.

23. W. Fan, S. B. Peh, Z. Zhang, H. Yuan, Z. Yang, Y. Wang, K. Chai, D. Sun and D. Zhao, *Angew. Chem. Int. Ed.*, 2021, **60**, 17338-17343.

24. J. Li, L. Jiang, S. Chen, A. Kirchon, B. Li, Y. Li and H.-C. Zhou, *J. Am. Chem. Soc.*, 2019, **141**, 3807-3811.

25. J. Pei, K. Shao, J.-X. Wang, H.-M. Wen, Y. Yang, Y. Cui, R. Krishna, B. Li and G. Qian, *Adv. Mater.*, 2020, **32**, 1908275.

26. T. Ke, Q. Wang, J. Shen, J. Zhou, Z. Bao, Q. Yang and Q. Ren, *Angew. Chem. Int. Ed.*, 2020, **59**, 12725-12730.

27. J. Shen, X. He, T. Ke, R. Krishna, J. M. van Baten, R. Chen, Z. Bao, H. Xing, M. Dincă, Z. Zhang, Q. Yang and Q. Ren, *Nat. Commun.*, 2020, **11**, 6259.

28. S.-i. Noro, R. Kitaura, M. Kondo, S. Kitagawa, T. Ishii, H. Matsuzaka and M. Yamashita, *J. Am. Chem. Soc.*, 2002, **124**, 2568-2583.